LJMU Research Online

Mao, Q, Wang, Y, Zhang, X, Zhao, X, Zhang, G and Mushayi, K

 Clarity method of fog and dust image in fully mechanized mining face

http://researchonline.ljmu.ac.uk/id/eprint/16536/

Article

Clarity method of fog and dust image in fully mechanized mining face

Qinghua Mao[1,2] · Yufei Wang[1,2] · Xuhui Zhang[1,2] · Xiaoyong Zhao[3] · Guangming Zhang[4] · Kundayi Mushayi[1,2]

Abstract

At present, the abnormal state of equipment and surrounding rocks in the fully mechanized mining face is mainly detected by visual methods. However, the vision sensor works in a low-light environment and it is affected by factors such as water fog and dust, which lead to blurred images. The defogging algorithm of image based on boundary constraint and context regularization has a good effect on image restoration in the daily environment, but the recovery quality is poor in low illumination environment. Therefore, a method based on boundary constraint and nonlinear context regularization is proposed. The model of fog and dust image is established, and the transmittance function is roughly estimated by boundary constraint method. Then, the nonlinear context regularization method based on logarithmic transformation is used to estimate and optimize the scene transmission model to improve the brightness of the image, and the low illumination fog and dust image is restored by the optimized transmittance function. The logarithmic transformation multiple is selected according to the peak value of image brightness. In order to highlight the effectiveness of our method, the widely used and improved Dark Channel Prior or other methods are used for comparison. The experiment results indicate that our method can effectively remove fog and dust and improve the brightness of the image of the fully mechanized face. It is of great significance to ensure safe production and safety of workers and equipment in coal mine.

Yufei Wang
562129353@qq.com

Qinghua Mao
maoqh@xust.edu.cn

Xuhui Zhang
zhangxh@xust.edu.cn

Xiaoyong Zhao
344170166@qq.com

Guangming Zhang
g.zhang@ljmu.ac.uk

Kundayi Mushayi
kundayimushayi@gmail.com

[1] School of Mechanical Engineering, Xi'an University of Science and Technology, Xi'an 710054, China

[2] Shaanxi Key Laboratory of Mine Electromechanical Equipment Intelligent Monitoring, Xi'an 710054, China

[3] Xi'an Heavy Equipment Intelligent Mine Engineering Technology Co.Ltd., Xi'an 710000, China

[4] Faculty of Engineering and Technology, General Engineering Research Institute, Liverpool John Moores University, Liverpool, UK

1 Introduction

With the development of intelligent monitoring technology, traditional coal mines have gradually transformed to intelligent coal mines with little or no people. The machine vision technology in coal mines is becoming more and more widespread. Real-time monitoring of working conditions is achieved by acquiring images of working faces. However, the working environment of the fully-mechanized working face is harsh and complicated, and a large amount of dust is generated during the production process. At the same time, the spray dust-falling equipment in coal mine generates a large amount of fog and water droplets, which greatly interferes with the quality of image and makes it difficult to achieve accurate identification of abnormal status for equipment and working faces. Therefore, the clarity method of fog and dust images is of great significance to ensure safe production and safety of workers and equipment in coal mine.

In recent years, many defogging and enhancement methods of images are proposed, such as model-based sharpening algorithms, image enhancement-based sharpening

algorithms and learning optimization-based algorithms [1]. The model-based sharpening algorithm combines the prior knowledge to obtain a clear image based on the imaging mechanism of dust and fog image. The image enhancement-based sharpening algorithm uses a contrast enhancement function to improve the visual effects of images. The learning-based optimization algorithms have been applied in the field of machine vision and image processing, including convolutional neural networks and generative adversarial networks [2–4]. The defogging method based on physical models has been widely used. Ni et al. [5] proposed a defogging method based on linear intensity transform (LIT) and local property analysis (LPA) for adaptive illumination parameter estimation. Tan et al. [6] proposed an image defogging method based on statistical rules, which successfully removed the fog of the images. However, the colors of the recovered image is oversaturated by this method. Fang et al. [7] proposed a variational model by combining the reformulation of the haze model and priors. But this method is not very effective in dense fog conditions. Fatal [8] proposed independent component analysis (ICA) method to estimate the scene and obtain a fog-free image. But this method is based on color information and is not suitable for grayscale images and dense fog weather conditions. Yang [9] proposed an adaptive decomposition method, which is a preprocessing method. It decomposes the image according to the transmission mapping value of the image, and reduces the influence of noise. He et al. [10] proposed the dark channel prior (DCP) method, but it has the disadvantages of long processing time and color distortion. Galdran [11] proposed a image dehazing technique that can remove the visual degradation due to haze without relying on the inversion of a physical model of haze formation. Huang et al. [12] proposed three subsequent optimization processes: depth of field estimation, color analysis and visual restoration, which made the prior law of dark channel suitable for image defogging in severe weather. However, too bright or too dark conditions will affect the stability of this method. He et al. [13] used guided filtering to obtain refined transmission at high speed, but the image processing effect in some special environments was not good. Ehsan et al. [14] proposed a new strategy is adopted to compute the dual transmission maps using the dark channel and atmospheric light, the transmission maps are refined to remove any remaining ill effects by using the gradient-domain-guided filter. Berman et al. [15] proposed a method for calculating the air-light which relies on the haze-lines prior that was recently introduced. This prior is based on the observation that the pixel values of a hazy image can be modeled as lines in RGB space that intersect at the air-light. Rong et al. [16] used wavelet transform to remove fog, and adjusted the approximate coefficient of wavelet transform to reduce noise and halo effect, but it could not improve the visibility of image under the condition of nonuniform fog. Zhang et al. [17] proposed a method of significance detection based on super-pixel intensity contrast, and set an adaptive upper bound for scene brightness to prevent some areas from being too bright. However, this method does not perform well in low brightness environment. Salazar et al. [18] proposed a computationally effective defogging method based on morphological operations and Gaussian filtering, which provides better defogging effect in the case of uniform fog, but has a poor image processing effect on the dense fog. Wang et al. [19] improved the DCP method by combining Fourier filtering and Gaussian filtering, and improved the operation speed of image restoration, but there are still limitations in dealing with low brightness environment. Zhang et al. [20] proposed an image defogging algorithm combining multiscale convolution network model and multiscale Retinex, which can effectively restore the image without fog.

The above-mentioned defogging method is relatively mature, but it is often devoted to defogging under ordinary atmospheric environment. However, the fog and dust are more severe than ordinary atmospheric environment in the fully mechanized working face environment. In addition, the fully mechanized mining face has the disadvantages of low lighting brightness. The fully mechanized mining face mostly uses fluorescent lamps and incandescent lamps, while LED is mostly used for portable miner's lamps. Moreover, because the lighting devices are only arranged on hydraulic support, and obscured by the hydraulic support, which will lead to insufficient lighting and low illumination in some places of fully mechanized mining face.

The existing defogging method cannot be well applied to the actual working environment of fully mechanized mining face. In this paper, our main contribution is to propose a clarity method of the fog and dust image of fully mechanized mining face based on boundary constraints and nonlinear context regularization, and logarithmic transformation is used to improve image brightness. First, a boundary constraint method is used to establish a rough estimation model of image scene transmittance. Then, the established scene transmittance model is optimized by constructing the weighting function using a nonlinear context regularization method based on logarithmic transformation. The brightness of the image is improved by logarithmic transformation. At the same time, the logarithmic transformation multiple is selected according to the peak value of image brightness. Finally, the image of fully mechanized mining face is cleared by the optimized scene transmittance. This method can greatly improve the brightness of the image, and realize the clarity of fog and dust image of fully mechanized mining face. It lays a good foundation for the identification of abnormal conditions for equipment and surrounding rocks in a fully mechanized mining face, and it is of great significance to ensure safe production of coal mine.
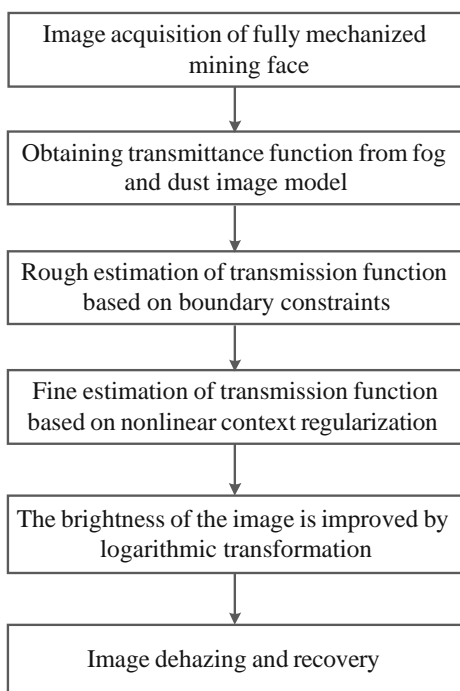
Fig. 1 The clarity scheme of fog and dust image

2 Clarity scheme of fog and dust image

The method is applied to clear low-light fog and dust images of fully mechanized mining faces. The clarity scheme of fog and dust image is presented in Fig. 1.

The working principle of clarity method of fog and dust image under the condition of low illumination in the fully mechanized mining face is as follows:

(1) Visual sensors are arranged on the hydraulic support to collect images of the fully mechanized mining face.
(2) The transmittance function model of fog and dust image is established based on the principle of fog and dust image formation.
(3) The boundary constraint method is used for rough estimation of the transmittance function.
(4) The nonlinear context regularization method is used for fine estimation of the transmittance function.
(5) The brightness of the image is improved by logarithmic transformation. At the same time, the logarithmic transformation multiple is selected according to the peak value of image brightness.
(6) The fog and dust image in fully mechanized face is restored, and the brightness enhancement of the image is realized.

3 Clarity method of fog and dust image of the fully mechanized mining face

3.1 Model of fog and dust image

During the propagation of light, due to the scattering of solid particles and liquid droplets in the air, the direction of the light is deviated, which leads to the intensity of the light to increase or decrease. In the fully mechanized mining face, the influence of dust and fog on the image is more serious than in the atmospheric environment. However, the principle is the same, and it can also be analyzed by the model of the fog and dust image in the atmospheric environment. Because, the fully mechanized mining face is not a closed indoor environment, which communicates with the ground atmosphere environment through the ventilation system. Therefore, its atmospheric scattering is similar to the atmospheric environment. The atmospheric scattering model is the main physical model for describing foggy images, which is presented in Eq. (1).

$$I(x) = t(x)J(x) + (1 - t(x))A \tag{1}$$

where $I(x)$ is a foggy image, $J(x)$ is a fog-free image, A is the global atmospheric light, A is generally considered to be constant, $t(x)$ is the scene transmittance function.

Assuming that the fog is homogeneous, the scene transmittance $t(x)$ is presented in Eq. (2):

$$t(x) = e^{-\beta d(x)} \tag{2}$$

where β is the extinction coefficient of the medium, $d(x)$ is the depth of field.

$t(x)J(x)$ is the direct attenuation term, which indicates the part of the reflected light attenuated by the scattering effect when it propagates in the medium. $(1 - t(x))A$ is the ambient light or the atmosphere. Light curtain represents the part of ambient light enhanced due to scattering during the propagation of the medium.

3.2 Rough estimation of transmission function based on boundary constraints

Equation (1) is a fog and dust image formation model, which shows that for any pixel x in RGB color space, the corresponding vectors A, $I(x)$ and $J(x)$ are co-planar, and their endpoints are colinear. From a single pixel, according to Eq. (1), if this pixel x is foggy, then the gray value $I(x)$ of this pixel x will be pushed to the global atmospheric light A. The larger the fog and dust, the closer the gray value $I(x)$ of the pixel x to A is. The defogging process is to linearly extrapolate along the direction of A to $I(x)$ to restore the
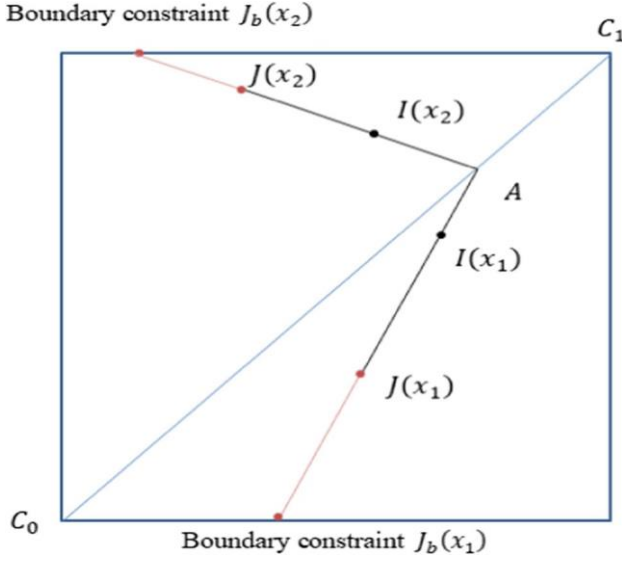
Fig. 2 Radiant cube and boundary constraints

fog-free image $J(x)$. The expression for linear extrapolation is presented in Eq. (3).

$$\frac{1}{t(x)} = \frac{J(x) - A}{I(x) - A} \tag{3}$$

The scene radiation of an image is always bounded, which is presented in Eq. (4):

$$C_0 \leq J(x) \leq C_1, x \in \tag{4}$$

where C_0 and C_1 are two constant vectors associated with image.

Because of any pixel x, the extrapolation of $J(x)$ must be located in the radiation cube, which is composed of C_0 and C_1 boundary points. Otherwise, the physical model of the fog image is violated. The radiant cube and boundary constraints are presented in Fig. 2.

Conversely, the boundary constraint on $J(x)$ can be transformed into the boundary constraint of $t(x)$. It is assumed that the global atmospheric light A is known, so that for any pixel x, we can calculate the corresponding boundary constraint point $J_b(x)$ as shown in Fig. 2. The lower bound of $t(x)$ can be determined by Eqs. (3) and (4). Finally, the following boundary constraint on $t(x)$ can be obtained by Eq. (5).

$$0 \leq t_b(x) \leq t(x) \leq 1 \tag{5}$$

where $t_b(x)$ is the lower bound of $t(x)$, which is presented in Eq. (6):

$$t_b(x) = \max_{c \in \{r,g,b\}} \frac{A^c - I^c(x)}{A^c - C_0^c}, \frac{A^c - I}{A^c - C} , 1 \tag{6}$$

where $I^c(x)$, A^c, C_0^c and C_1^c are the color channels of I, A, C_0 and C_1, respectively.

In the dark channel prior, assuming $C_0 = 0$, the gray value of the A is greater than the gray value of any pixel in the foggy image. Assuming that the gray value of the dark channel based on a single pixel of $J(x)$ is 0, $t_b(x)$ of the dark channel prior method can be directly calculated by Eq. (1).

According to reference [20], the block-based transmittance $\tilde{t}(x)$ is presented in Eq. (7):

$$\tilde{t}(x) \quad \min_{y \in \omega_x} \max_{z \in \omega_y} t_b(z) \tag{7}$$

where ω_x is a local block centered on x, and ω_y is a local block centered on y.

Equation (7) describes the local minimum filtering with x as the center to obtain the local minimum coordinate point y, and then the local maximum filtering with y as the center to obtain the local maximum coordinate point z. The gray value of coordinate point z is as the gray value of the new transmittance $\tilde{t}$ at the x point. By directly performing the closing operation in morphology on $t_b(x)$, a new transmittance $\tilde{t}(x)$ can be obtained by Eq. (7).

3.3 Fine estimation of transmittance function based on nonlinear context regularization

The principle of restoring for fog and dust images in a fully mechanized mining face is similar to the restoration of fog images in the atmospheric environment. The nonlinear context regularization has a significant effect on the restoration of fog images. However, the core is to construct a weighting function to obtain the optimal solution to achieve image dehazing. In addition, the fog and dust in the fully mechanized mining face are serious and the light intensity is insufficient, so it is important to construct a reasonable weighting function. Weighting function $W(x, y)$ is presented in Eq. (8).

$$\min_{x,y} W(x, y)(t(y) - t(x)) \tag{8}$$

where x and y are two adjacent pixels. The smaller the $W(x, y)$, the smaller the corresponding context constraint of the transmittance $t(x)$ between the pixels x and y;

A weighting function is constructed by calculating the brightness difference between adjacent pixels, and a logarithmic transformation is introduced, which is presented in Eq. (9).
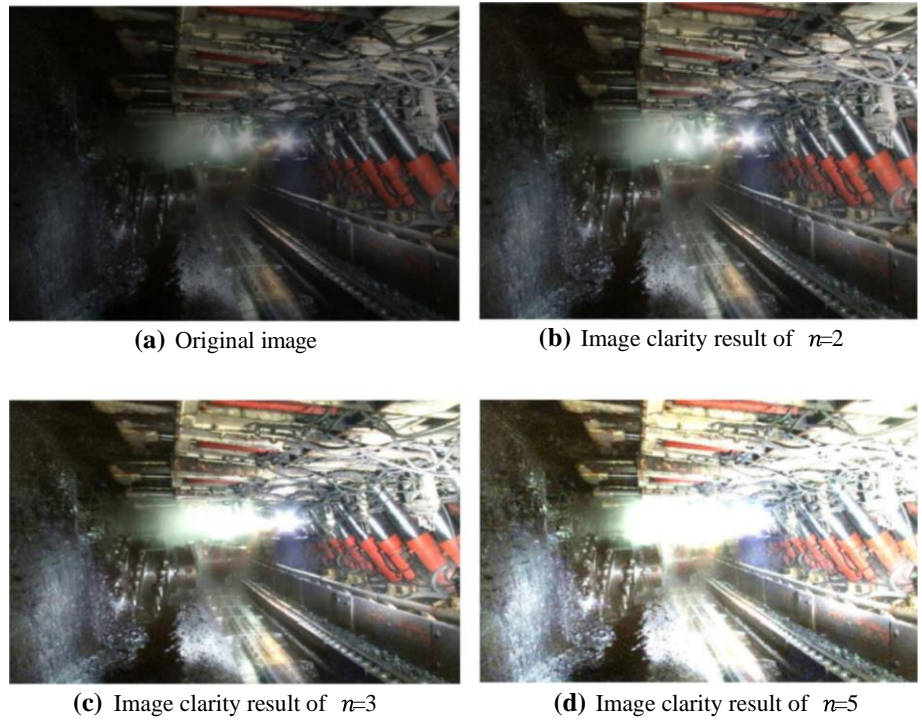
$$W(x, y) = |\log(x) - \log(y)|^a + \varepsilon^{-1} \tag{9}$$
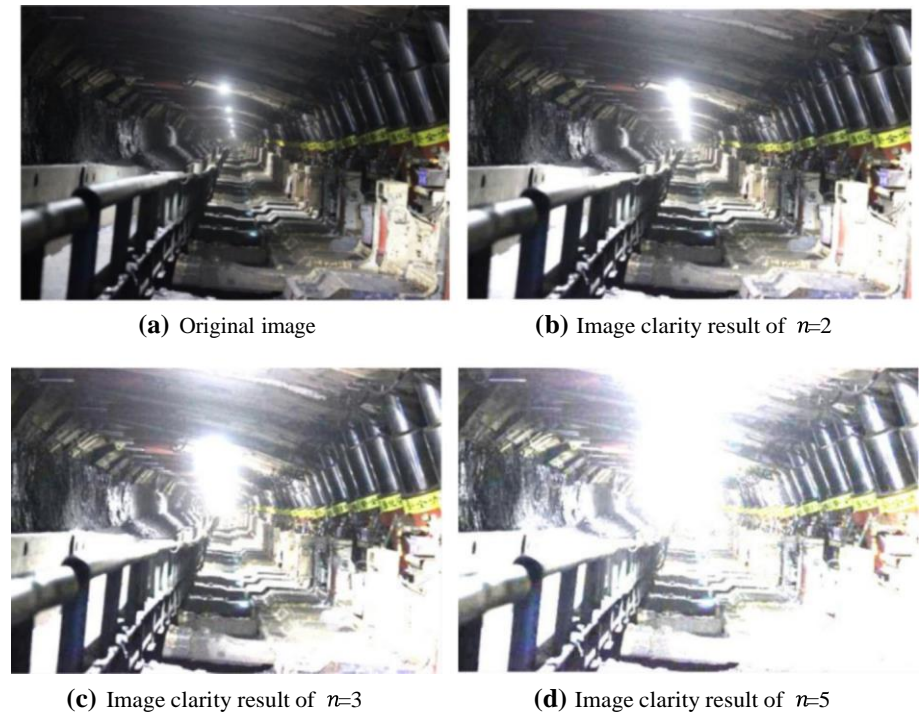
where $\log(x)$ is the logarithm of the brightness channel of
image $I(x)$, the index $a > 0$, which is used to control the

(a) Original image

(b) Image clarity result of *n*=2

(c) Image clarity result of *n*=3

(d) Image clarity result of *n*=5

(a) Original image

(b) Image clarity result of *n*=2

(c) Image clarity result of *n*=3

(d) Image clarity result of *n*=5

brightness difference and sensitivity of two adjacent pixels. ε is usually taken as 0.0001, which is used to prevent the occurrence of 0 in the denominator [21].

By introducing 8 Kirsch operators and 1 Laplacian operator and rewrite Eq. (9), which is presented in Eq. (10).
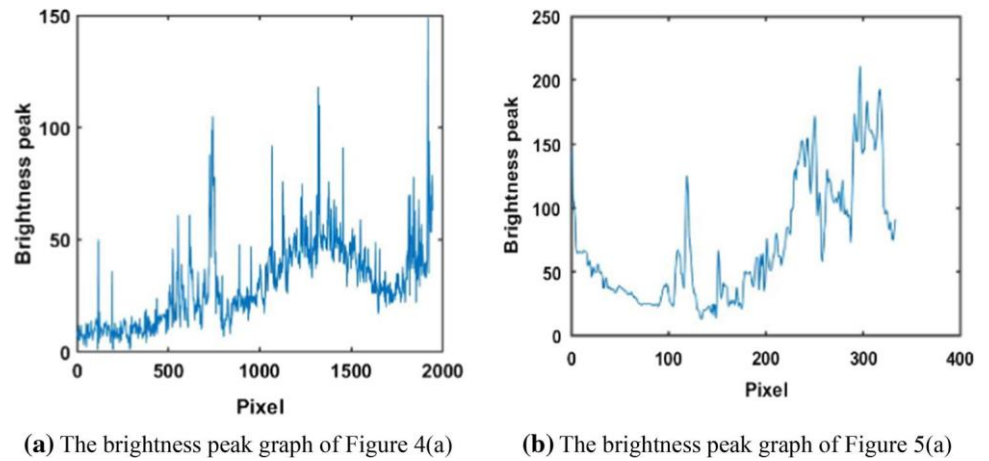
$$W_j(i) = \left[D_j \underset{\otimes}{} \left| \log(x) - \log(y) \right|^a + \varepsilon \right]^{-1} \tag{10}$$

where $W_j(i)$ is the weight matrix and D_j is the introduced difference operator.

Therefore, the optimized transmittance function $t(x)$ can be obtained from Eq. (11).

$$\min_t \frac{\lambda}{2} \|t - \tilde{t}\|_2^2 + \sum_{j \in \omega} \| W_j \cdot (D_j \otimes t) \|_1 \tag{11}$$

13

Fig. 5 The brightness peak maps of Figs. 4a and 5a

(a) The brightness peak graph of Figure 4(a)   **(b)** The brightness peak graph of Figure 5(a)

where the first part is the data fidelity term, which is used to measure the fidelity between $t(x)$ and the block-based transmittance $t^{\tilde{}}(x)$ based on the boundary constraint. The second part is the context constraint of $t(x)$, that is the regularization term of the objective function, and that is used to constrain the ill-posedness of the restoration problem. λ is a regularization parameter for balancing the data fidelity and regularization terms.

According to the solution process in the reference [9], an alternating minimization algorithm is used to solve the objective function. For a fixed β, the objective function is solved by optimizing u_j and t alternately. The optimization results is presented in Eq. (12).

$$t^* = \mathrm{FFT}^{-1} \beta \frac{\frac{\lambda}{\beta} \mathrm{FFT} \ t^{\tilde{}} + \sum_{j\in\omega} \overline{\mathrm{FFT} \ D_j} \cdot \mathrm{FFT} \ u_j}{\frac{\lambda}{\beta} + \sum_{j\in\omega} \overline{\mathrm{FFT} \ D_j} \cdot \mathrm{FFT} \ D_j} \quad (12)$$

where FFT is a Fourier transform, FFT^{-1} is an inverse Fourier transform, $\overline{()}$ represents a complex conjugate, and $\cdot$ represents a matrix point multiplication, β is a weight, u_j is the auxiliary variable.

3.4 Image brightness enhancement based on logarithmic transformation

In the ordinary atmospheric environment, the above methods have completed a detailed estimation of the transmittance function, and a fog-free image can be obtained. However, the fully mechanized mining face is different from ordinary atmospheric environment. In the fully mechanized mining face, the vision sensor works in a low-light environment and it is affected by factors such as water fog and dust, which lead to blurred images.

Based on the above problems, the logarithmic transformation is used to improve the image brightness. The expression for logarithmic transformation is presented in Eq. (13). Gen-

erally, the base number of logarithmic transformation is generally 10, that is, the common logarithm is used for logarithmic transformation.

$$t = n * \lg(c + 1) \quad (13)$$

where t is the output gray value, n is the conversion multiple, and c is the original gray value.

3.5 The logarithmic transformation multiple selected according to the peak value of image brightness

We selects the logarithm transform multiple according to the peak value of image brightness. When the maximum luminance of the image is less than 100, we can choose n more than 4 to restore. When the maximum brightness of the original image is between 100 and 200, we can choose logarithmic transformation multiple n as 3 to restore. When the maximum brightness of the image is between 200 and 300, we can choose logarithmic transformation multiple n as 2 to restore. When it is higher than 300, the brightness of image can be regarded as normal and we chose the logarithmic transformation multiple n as 1.

In order to verify the method, we chose different logarithmic transformation multiple n to test the restoration effect of image in the fully-mechanized working face. The results are presented in Figs. 3 and 4, and the brightness peak graph of Figs. 3a and 4a is presented in Fig. 5.

As can be observed in Fig. 4, it has the best visual effect with the logarithm transform multiple n as 3. It has the best visual effect with the logarithm transform multiple n as 2 in Fig. 5. According to the brightness peak graph of Fig. 6, the logarithm transform multiple n is selected as 3 in Fig. 4, and the logarithm transform multiple n is selected as 2 in Fig. 5. The results indicate that we can effectively avoid the problem that the image is too bright after restoration by selecting the

Fig. 6 Comparison of image clarity results using different methods

(**a**) Original image

(**b**) Brightness peak graph

(**c**) proposed

(**d**) He
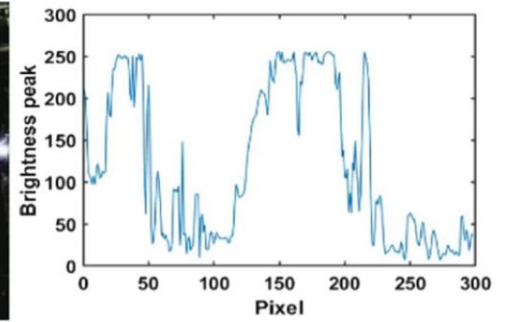
(**e**) Meng

(**f**) Galdran

(**g**) Ehsan

(**h**) Berman

Fig. 7 Comparison of image clarity results using different methods

(a) Original image

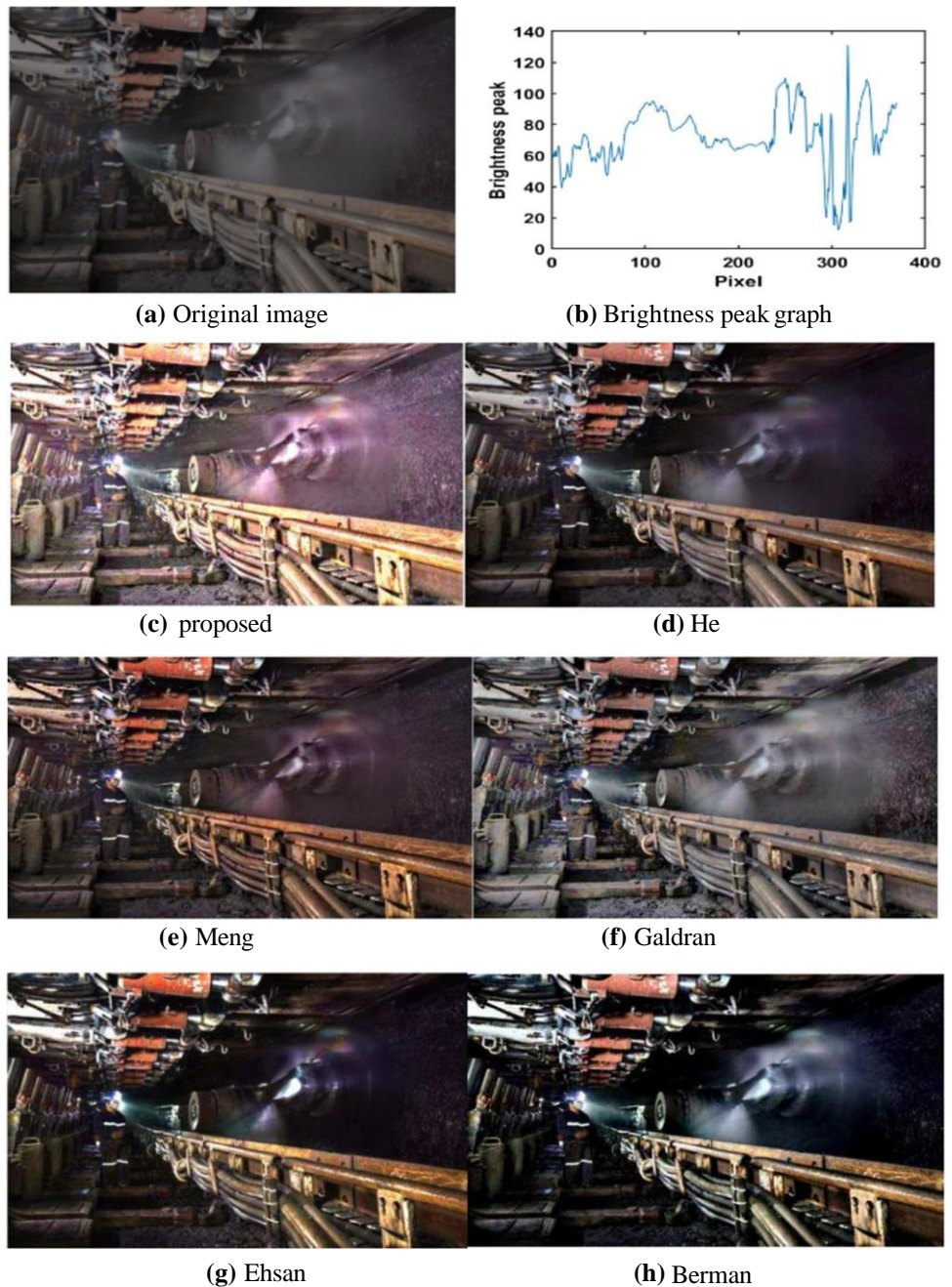(b) Brightness peak graph

(c) proposed

(d) He

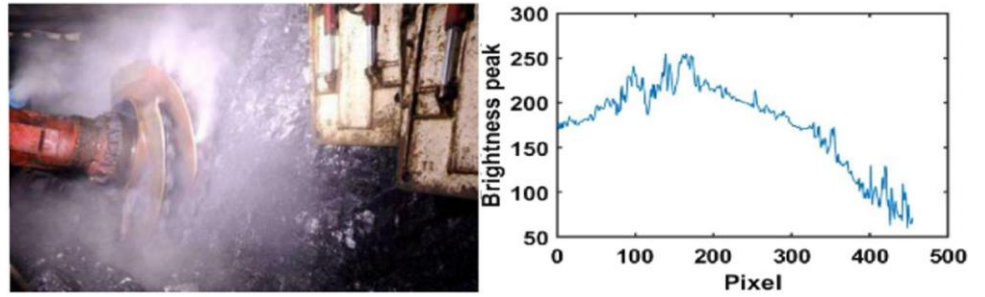(e) Meng

(f) Galdran

(g) Ehsan

(h) Berman

logarithmic transformation multiple according to the peak value of image brightness.

3.6 Image dehazing and recovery

According to the atmospheric scattering model proposed by Eq. (1), the fog-free image $J(x)$ is restored from the known observed fog-dust image $I(x)$. In addition to the transmission function $t(x)$, the global atmospheric light A needs to be estimated. Meng et al. [21] first filter each channel of the input image to obtain three dark channel images, and then take the maximum gray value of RGB three dark channels as the gray value of atmospheric light a in this channel. He et al. [10] first solved the input channel I for its dark channel image I_{dark} and selected the brightest pixels at 0.1% of the total number of pixels in the image I_{dark}. According to the coordinates of these pixel points, find the pixel point with the largest sum of these pixel points in the three channels of the original image I. The three-channel gray value of this point is used as the three-channel gray value of atmospheric light A. We can also select the most serious fog pixels as atmospheric light A in the fog image by the artificial method. This method is the

Fig. 8 Comparison of image clarity results using different methods

(a) Original image

(b) Brightness peak graph

(c) proposed

(d) He

(e) Meng

(f) Galdran

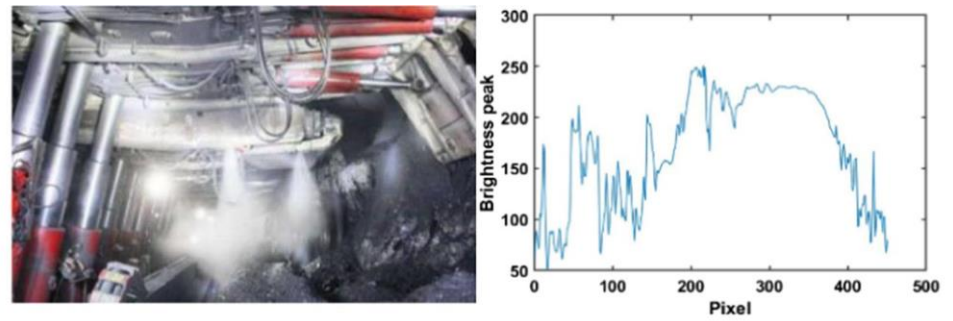
(g) Ehsan

(h) Berman

most accurate, but it needs human interaction and cannot be automated.

Once $t(x)$ and A are obtained, a fog-free image can be obtained by Eq. (14).

$$J(x) = \frac{I(x) - A}{[\max(t(x), \varepsilon)]^{\delta}} + A \qquad (14)$$

where ε is usually taken as 0.0001 to prevent the denominator from appearing as 0, and δ is equivalent to the medium extinction coefficient in Eq. (2), which is used to fine-tune the defogging effect.

Fig. 9 Comparison of image clarity results using different methods

(**a**) Original image

(**b**) Brightness peak graph

(**c**) proposed

(**d**) He

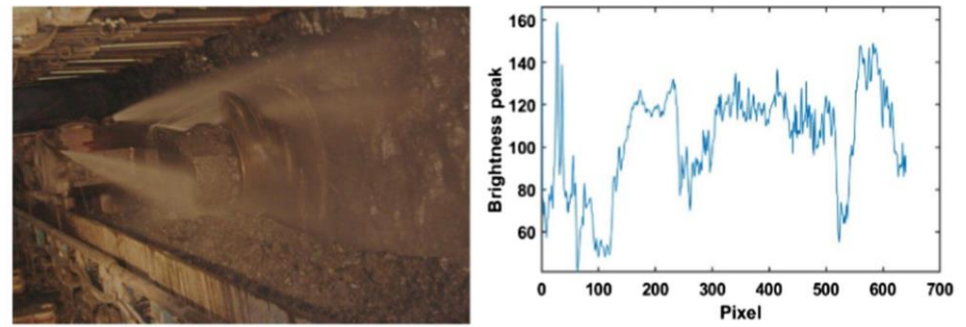(**e**) Meng

(**f**) Galdran

(**g**) Ehsan

(**h**) Berman

4 Results analysis and discussion

4.1 Results analysis

To verify the defogging and enhancement effects of clarity method of fog and dust image under the condition of low illumination in fully mechanized mining face, different methods are used to restore the image of fully mechanized mining face, and the contrast results are presented in Figs. 6, 7, 8, 9, 10 and 11. In Figs. 6, 7, 8, 9, 10 and 11, Figure (a) is the original image. Figure (b) is the brightness peak graph. Figure(c) is the processing result of ours. Figures (d) to (h)

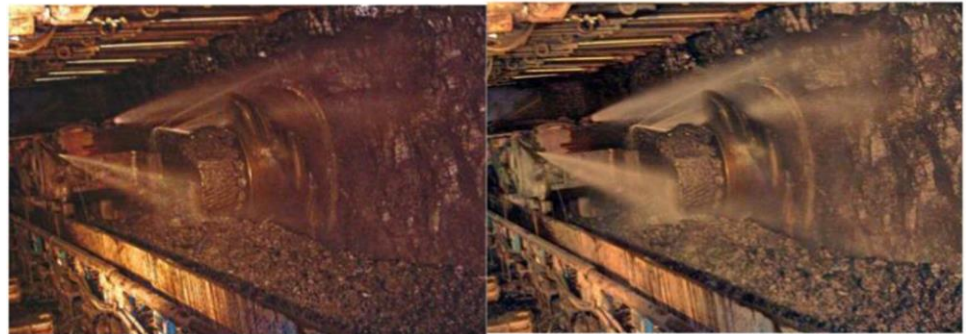**Fig. 10** Comparison of image clarity results using different methods

(a) Original image

(b) Brightness peak graph

(c) proposed

(d) He

(e) Meng

(f) Galdran

(g) Ehsan

(h) Berman

are the processing results of the methods of He [10], Meng [21], Galdran [11], Ehsan [14] and Berman [15]. According to the brightness peak graph of each image, the brightness peaks of Figs. 6, 8, 9 and 11 are between 200 and 300, and the brightness peaks of Figs. 7 and 10 are between 100 and 200.

Therefore, the logarithm transformation multiple is selected as n for 2 in Figs. 6, 8, 9 and 11, and the logarithm transformation multiple is selected as n for 3 in Figs. 7 and 10.

In order to reflect the processing effect of this method on fog and dust image of fully mechanized mining face, the

Fig. 11 Comparison of image clarity results using different methods

(a) Original image

(b) Brightness peak graph

(c) proposed

(d) He

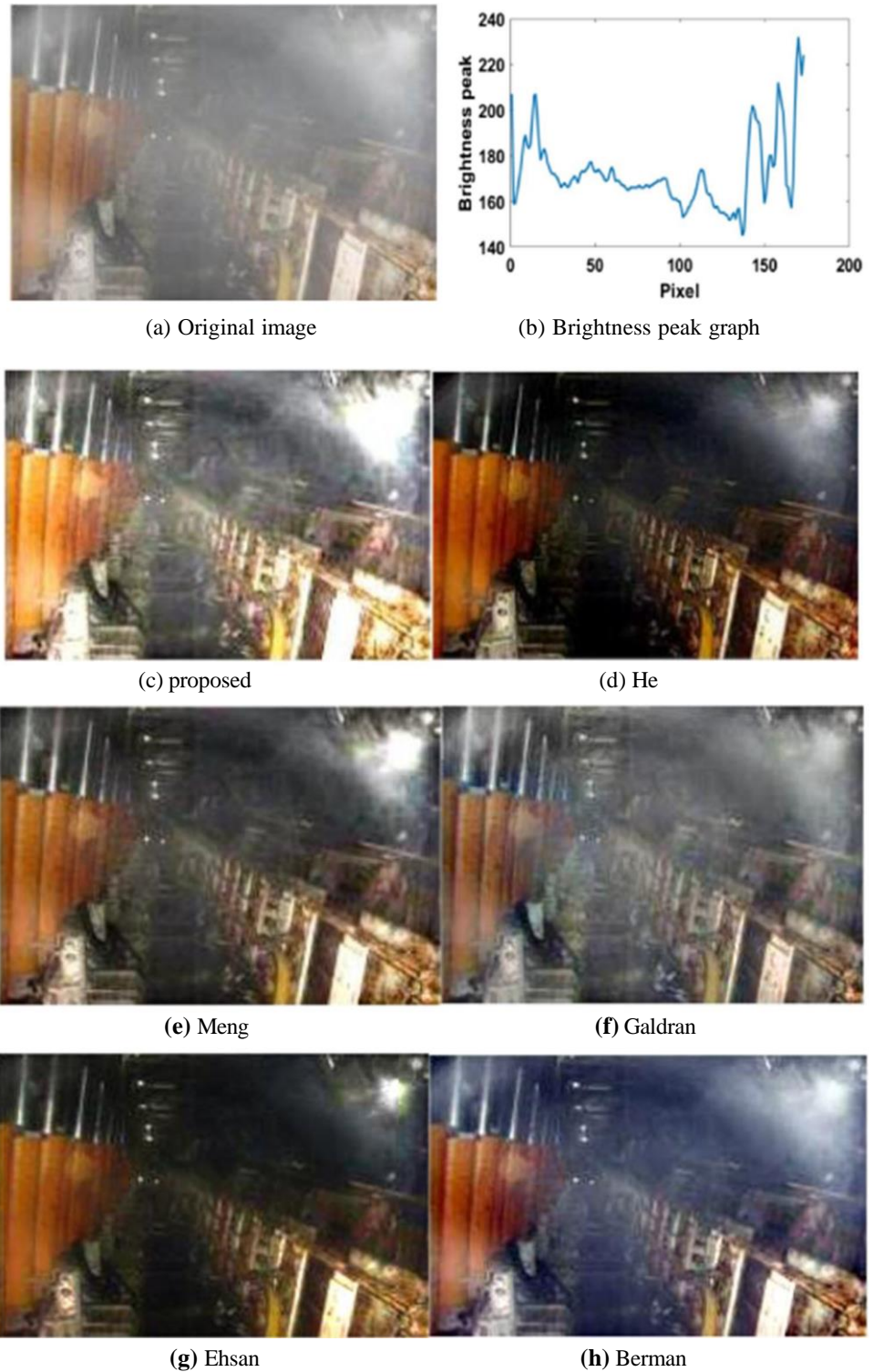(e) Meng

(f) Galdran

(g) Ehsan

(h) Berman

Peak Signal-to-Noise Ratio (PSNR) and information entropy are selected as objective evaluation indicators. PSNR is a commonly used objective evaluation index of images. There is a positive correlation between image clarity and PSNR. Information entropy reflects the diversity of gray value of
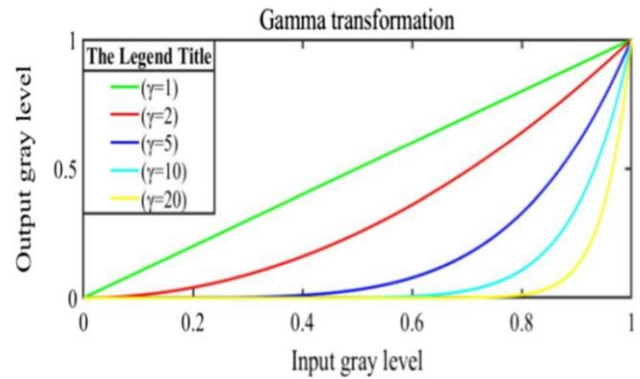
image. The comparison of image clarity results of different methods is presented in Table 1.

Figure 6 is an image of the cutting process of shearer, the main fog and dust of image are concentrated in the drum of shearer. In the Figure, other methods have good effect on removing the fog and dust. However, the brightness of

Table 1 PSNR and information entropy of different methods

Figs.	Methods	PSNR	Information entropy
Figure 6	Proposed	18.346	7.648
	He	17.056	7.624
	Meng	14.290	7.490
	Galdran	18.231	7.634
	Ehsan	12.145	7.397
	Berman	12.292	6.988
Figure 7	Proposed	16.337	7.679
	He	13.772	7.199
	Meng	16.298	7.043
	Galdran	16.731	7.518
	Ehsan	14.637	6.971
	Berman	13.939	6.591
Figure 8	Proposed	16.949	7.732
	He	11.274	7.615
	Meng	11.238	7.518
	Galdran	14.612	7.751
	Ehsan	9.758	7.424
	Berman	10.331	7.330
Figure 9	Proposed	15.522	7.770
	He	13.074	7.620
	Meng	10.732	7.472
	Galdran	15.515	7.708
	Ehsan	10.231	7.355
	Berman	9.142	6.833
Figure 10	Proposed	18.703	7.437
	He	18.092	7.274
	Meng	17.457	6.913
	Galdran	18.382	7.342
	Ehsan	12.697	6.653
	Berman	14.084	7.140
Figure 11	Proposed method	16.882	7.551
	He	8.885	7.176
	Meng	12.137	7.297
	Galdran	15.077	7.102
	Ehsan	8.945	6.903
	Berman	13.352	7.486

Fig. 12 Gamma transformation function curve

uation indicators are also highest, which is consistent with the visual observation. Figure 8 is a detailed image of cutting drum of shearer. The lower half of the coal wall is unclear in DCP method, which shows that the detail of DCP method is insufficient under the condition of high fog and dust. In our method, all areas of the middle coal wall are clearly visible, and the details are more abundant. The PSNR value is greatly improved due to the increase of brightness, and information entropy also increases with the increase in information in the image. Figure 9 is an image of a roadway in a fully mechanized mining face. There is mainly interference from light and fog. The other method is not effective, the influence of light and fog still exists and the brightness is reduced, especially Figure (g) and Figure (h). The brightness of ours has increased and coal walls, coal blocks and hydraulic supports in the figure are more clearly, the evaluation index also performs better. Figure 10 is an image of cutting process of the shearer. The brightness of the original image is high, so He and Galdran's method have a good visual effect. In Fig. 11, the fog and dust is very serious, and the image quality is greatly disturbed, therefore, the results of other methods are visually poor. But our method performs best in visual effect and evaluation index, PSNR is much higher than others. After processing the image by our method, the logarithmic transformation effectively solves the problem of insufficient brightness, the PSNR and information entropy of our method are higher than other methods, and more detailed information can be observed.

Subjectively, compared with the results of the other methods, the brightness of our method can be improved, and more details of coal wall and equipment are apparent. At the same time, our method has a better effect on defogging and brightness improvement. It is more suitable for image defogging in the fully mechanized mining face environment. The image quality can better meet the needs of actual working conditions. It is shown in Table 1 that the PSNR and information entropy are the maximum by using our method, which indicate that our method has better effect on processing the fog
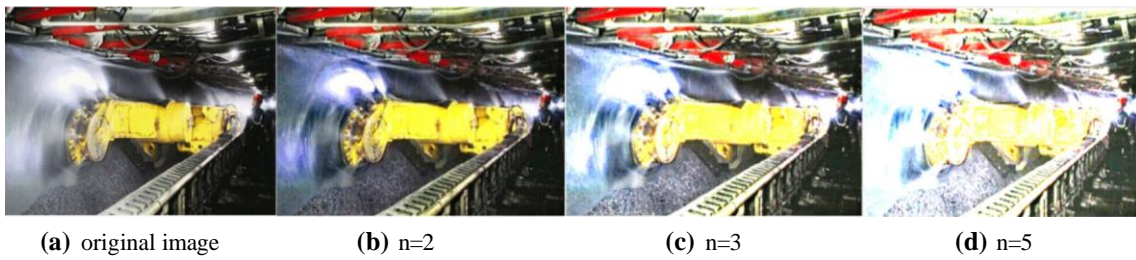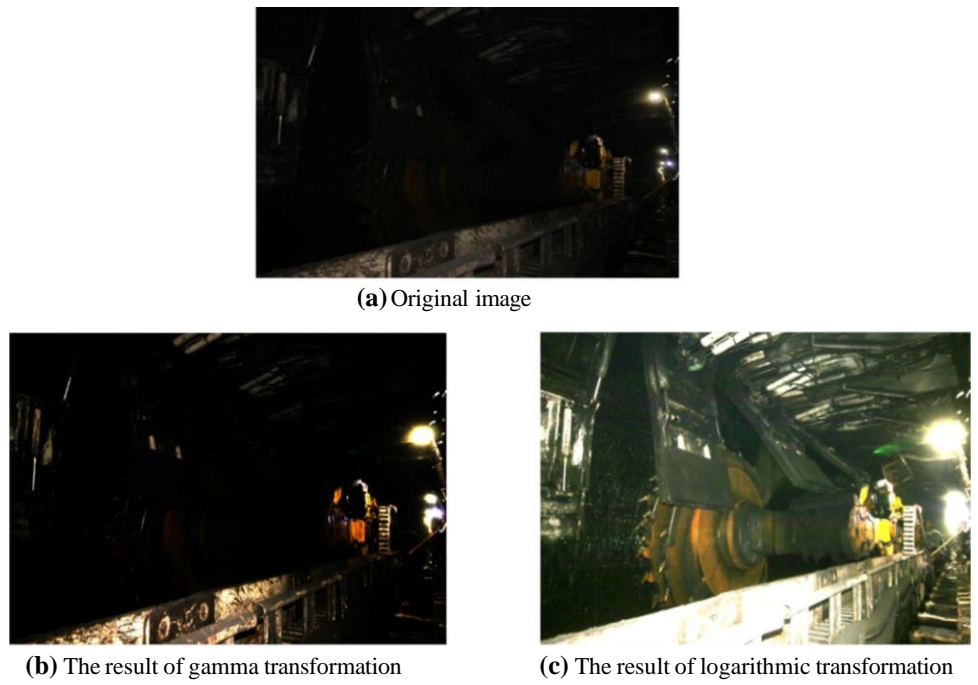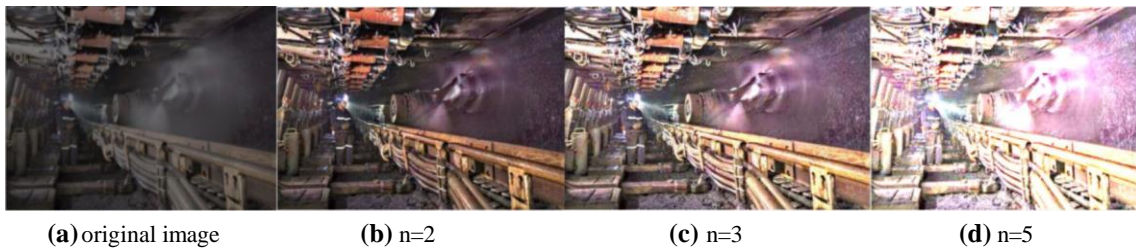
these results is still insufficient. In our method, the coal wall near the drum is more clearly and the color is more full. Meanwhile, PSNR and information entropy have been greatly improved. Figure 7 is an image of the cutting process of shearer. The defogging effect of Figure (d) and Figure (e) is almost the same, but there is also a problem of lower brightness, and the result of Figure (g) and Figure (h) is very dark. But Galdran's method performs well, and the results are similar to ours. The coal wall is clearly exposed, such as hydraulic support, are also clearer to observe, and the eval-

Fig. 13 Results of gamma and log transformation processing

(a) Original image

(b) The result of gamma transformation

(c) The result of logarithmic transformation

(a) original image   **(b)** n=2   **(c)** n=3   **(d)** n=5

Fig. 14 Comparison results of different *n* in Fig. 6

(a) original image   **(b)** n=2   **(c)** n=3   **(d)** n=5

Fig. 15 Comparison results of different *n* in Fig. 7

(a) original image   **(b)** n=2   **(c)** n=3   **(d)** n=5
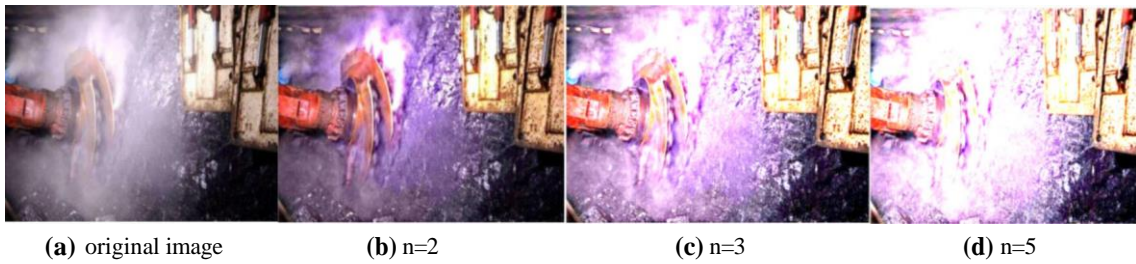
Fig. 16 Comparison results of different *n* in Fig. 8

and dust images of the fully mechanized mining face, it lays a foundation for the research of target recognition and detection in coal mine.

4.2 Discussion

Nonlinear transformation is the main means of brightness enhancement, which mainly includes gamma transformation and logarithmic transformation. We discuss the enhancement effect of logarithm transform and gamma transform in this section. The gamma transformation function curve is presented in Fig. 12. In order to compare the effect of gamma transformation and logarithmic transformation on the improvement of brightness, the image with lower brightness in the comprehensive mining face is used for verifying. The original image is presented in Fig. 13a. The result of logarithmic transformation is presented in Fig. 13b, and the result of gamma transformation is presented in Fig. 13c. As shown in Fig. 13, the image clarity result of logarithmic transformation is better than gamma transformation.

The gamma function curve shows the slope of the curve with the high grayscale value is larger, which indicates that the gamma transform has a poor enhancement effect on pixels with low grayscale values, and has a strong enhancement effect on pixels with high grayscale values. Comparing the image of two different nonlinear transformations and the actual enhancement effect, it can be seen that in the fully-mechanized working face, some high-illuminance areas appear in the image due to mining lights and equipment reflections. The gamma transformation has over-enhanced these areas, while other areas with lower brightness have poorer enhancement effects. This is consistent with the gamma function curve. While the logarithmic transformation avoids the problem that these parts are excessively enhanced, and improves the brightness of other low-illumination areas. Therefore, we use a logarithmic transformation to improve image brightness. This method is suitable for the actual working conditions of the fully mechanized mining face.

In order to vertify the influence of n on the final output result, we select different n to process Figs. 6, 7 and 8. The results are as shown in Figs. 14, 15 and 16, respectively.

When n is for 5, the images have been overexposed in Figs. 14, 15 and 16. In Fig. 14 and Fig. 16, the visual effect is the best when n is for 2, and when n is for 3, the image is too bright. In Fig. 15, when n is for 2, the brightness of the restored image is insufficient, but the effect of n for 3 is significantly better, and there is no over brightness. This is consistent with the experiment results in Sect. 4.1. The results indicate that n selected by the proposed method is effective.

5 Conclusions

Aiming at the problems of clarity for fog dust image with low brightness in the fully mechanized mining face, the clarity method of fog dust image based on boundary constraint and nonlinear context regularization, and the image brightness improvement based on logarithmic transformation is proposed. We found that under the condition of low illumination and dense fog of fully mechanized mining face, the logarithmic transformation is more suitable than the gamma transformation, which can improve the brightness of the image without over lighting. In the proposed method, the logarithm transformation multiple is selected based on the image brightness peak. In the experiment verification, the proposed defogging method is compared to some of the existing defogging methods. The contrast results indicate that the proposed method has the better clarity effectiveness and it is more suitable image clarity for the fully mechanized mining face environment. We will study the intelligent recognition of the abnormal state of equipment and surrounding rock for the fully mechanized working face based on this research.

References

1. Wang, W., Yuan, X.: Recent advances in image dehazing. IEEE CAA J. Autom. Sin. **4**(3), 410–436 (2017)
2. Zhang, Y., Ding, L., Sharma, G.: Hazerd: an outdoor scene dataset and benchmark for single image dehazing. In: IEEE international conference on image processing, pp. 3205–3209 (2017)
3. Yuan, K., Wei, J., Lu, W., et al.: Single image dehazing via NIN-DehazeNet. IEEE Access **7**, 181348–181356 (2019)
4. Li, C., Zhao, X., Zhang, Z., et al.: Generative adversarial dehaze mapping nets. Pattern Recogn. Lett. **119**, 238–244 (2019)
5. Ni, W., Gao, X., Wang, Y.: Single satellite image dehazing via linear intensity transformation and local property analysis. Neurocomputing **175**, 25–39 (2016)
6. Tan, R.T.: Visibility in bad weather from a single image. In: 2008 IEEE conference on computer vision and pattern recognition. IEEE, pp. 1–8 (2008)
7. Fang, F., Wang, T., Wang, Y., et al.: Variational single image dehazing for enhanced visualization. IEEE Trans. Multimed. **22**(10), 2537–2550 (2019)
8. Fattal, R.: Single image dehazing. ACM Trans. Graph. **27**(3), 1–9 (2008)
9. Yang, M., Liu, J., Li, Z., et al.: Pre-processing for single image dehazing. Signal Process. Image Commun. **83**, 115777 (2020)

10. He, K., Sun, J., Tang, X.: Single image haze removal using dark channel prior. IEEE Trans. Pattern Anal. Mach. Intell. **33**(12), 2341–2353 (2010)

11. Galdran, A.: Image dehazing by artificial multiple-exposure image fusion. Signal Process. **149**, 135–147 (2018)

12. Huang, S.C., Chen, B.H., Wang, W.J.: Visibility restoration of single hazyimages captured in real-world weather conditions. IEEE Trans. Circuits Syst. Video Technol. **24**(10), 1814–1824 (2014)

13. He, K., Sun, J., Xiaoou, T.: Guided image filtering. IEEE Trans. Pattern Anal. Mach. Intell. **35**(6), 1397–1409 (2013)

14. Ehsan, S.M., Imran, M., Ullah, A., et al.: A single image dehazing technique using the dual transmission maps strategy and gradient-domain guided image filtering. IEEE Access **9**, 89055–89063 (2021)

15. Berman, D., Treibitz, T., Avidan, S.: Air-light estimation using haze-lines. In: 2017 IEEE international conference on computational photography (ICCP). IEEE, pp. 1–9 (2017)

16. Rong, Z., Jun, W.L.: Improved wavelet transform algorithm for single image dehazing. Optik **125**(13), 3064–3066 (2014)

17. Zhang, L., Wang, S., Wang, X.: Saliency-based dark channel prior model for single image haze removal. IET Image Process. **12**(6), 1049–1055 (2018)

18. Salazar-Colores, S., Ramos-Arreguin, J.M., Echeverri, C.J.O., et al.: Image dehazing using morphological opening, dilation and Gaussian filtering. SIViP **12**(7), 1329–1335 (2018)

19. Wang, Z., Feng, Y.: Fast single haze image enhancement. Comput. Electr. Eng. **40**(3), 785–795 (2014)

20. Zhang, W., Dong, L., Pan, X., et al.: Single image defogging based on multi-channel convolutional MSRCR. IEEE Access **7**, 72492–72504 (2019)

21. Meng, G., Wang, Y., Duan, J., et al.: Efficient image dehazing with boundary constraint and contextual regularization. In: Proceedings of the IEEE international conference on computer vision, pp. 617–624 (2013)